J. Fluid Mech. (1997), *vol.* 339, *pp.* 121–142. Printed in the United Kingdom

On the effect of a central vortex on a stretched magnetic flux tube

By KONRAD BAJER† AND H. K. MOFFATT

Department of Applied Mathematics and Theoretical Physics, University of Cambridge, Silver Street, Cambridge CB3 9EW, UK

(Received 8 March 1996 and in revised form 6 February 1997)

Experiments and numerical simulations of fully developed turbulence reveal the existence of elongated vortices whose length is of the order of the integral scale of turbulence while the diameter is somewhere between the Kolmogorov scale and the Taylor microscale. These vortices are embedded in quasi-irrotational background flow whose straining action counteracts viscous decay and determines their cross-sectional shape. In the present paper we analyse the effect of a stretched vortex of this kind on a uni-directional magnetic flux tube aligned with vorticity in an electrically conducting fluid. When the magnetic Prandtl number is large, $P_m \gtrsim 1$, the field is concentrated in a flux tube which, like the vortex itself, has elliptical cross-section inclined at 45° to the principal axes of strain. We focus on the limit $P_m \ll 1$ when the magnetic flux tube has radial extent much larger than that of the vortex, which appears like a point vortex as regards its action on the flux tube. We find the steady-state solution valid in the entire plane outside the vortex core. The solution shows that the magnetic field has a logarithmic spiral component and no definite orientation of the inner contours. Such magnetized vortices may be expected to exist in MHD turbulence with weak magnetic field where the field shows a tendency to align itself with vorticity. Magnetized vortices may also be expected to exist on the solar surface near the corners of convection cells where downwelling swirling flow tends to concentrate the magnetic field.

1. Introduction

Vortex tubes, subjected to the action of a locally uniform straining motion and to the effect of viscous diffusion, were identified half a century ago (Burgers 1948) as a key ingredient of turbulent flow. The idea that at least the dissipative scales of turbulence might be well represented by a random distribution of vortex tubes and/or sheets was pursued by Townsend (1951) (see Batchelor 1953, §7.4), and has received much impetus from the frequent detection of concentrated vortices both in direct numerical simulation (DNS) of turbulence (see, for example, Vincent & Meneguzzi 1991; She, Jackson & Orszag 1990; Jimenez *et al.* 1993), and in experiments on turbulence in liquids seeded with small bubbles (Douady, Couder & Brachet 1991; Cadot, Douady & Couder 1995; Villermaux, Sixou & Gagne 1995). A high-Reynolds-number asymptotic theory of vortices subjected to the non-axisymmetric strain

$$\boldsymbol{U}^* = (\alpha x^*, \beta y^*, \gamma z^*), \qquad \alpha + \beta + \gamma = 0, \qquad \alpha \leqslant \beta \leqslant \gamma \tag{1.1}$$

† On leave from the Institute of Geophysics, University of Warsaw, Poland.

(where an asterisk denotes dimensional variables) has been developed by Moffatt, Kida & Ohkitani (1994, hereafter referred to as MKO94), and this explains certain features of the dissipation fields observed in such vortices in DNS (Kida & Ohkitani 1992). A parallel theory of two-dimensional unsteady vortices subjected to two-dimensional strain (Jiménez, Moffatt & Vasco 1996) explains the structure of the vortices that emerge in freely decaying two-dimensional turbulence (McWilliams 1984), and provides a new handle on the dynamics of the asymptotic ($t \to \infty$) high-Reynolds-number evolution.

The success of these approaches encourages an extension of the basic ideas to magnetohydrodynamic (MHD) turbulence, for which magnetic field $\boldsymbol{B}^*$, as well as vorticity $\boldsymbol{\omega}^*$, is subject to the orienting and intensifying effects of any local strain field. The powerful (though admittedly incomplete) analogy between $\boldsymbol{B}^*$ and $\boldsymbol{\omega}^*$ in the turbulence context was first exploited by Batchelor (1950) (see Moffatt 1978, §3.2); the analogy has been pursued for the problem of stretched 'vortex/magnetic flux tubes' or 'magnetic sinew' by Bajer (1995) who argues the case for simultaneous alignment of $\boldsymbol{B}^*$ and $\boldsymbol{\omega}^*$ along the axis Oz^* of greatest positive rate of strain. These fields are subject to different diffusivities – kinematic viscosity ν in the case of vorticity, and magnetic diffusivity η in the case of magnetic field; this means that for positive strain rate γ, the viscous and magnetic diffusion length scales δ_v and δ_m are different:

$$\delta_v = (\nu/\gamma)^{1/2}\,, \qquad \delta_m = (\eta/\gamma)^{1/2}\,. \tag{1.2}$$

We shall suppose in the present paper that the magnetic Prandtl number is small:

$$P_m = \nu/\eta = (\delta_v/\delta_m)^2 \ll 1 \tag{1.3}$$

and we shall focus attention on the structure of the magnetic field on scales $r^* \gg \delta_v$, at which the additional velocity field is essentially that due to a point vortex (see (1.13) below).

We shall suppose that the circulation associated with this vortex is $\Gamma(>0)$, and that the magnetic flux is $\Phi(>0)$, and that both Γ and Φ are finite. We may then adopt dimensionless variables

$$r = r^*/\delta_m\,, \qquad \psi = \psi^*/\Gamma\,, \qquad \boldsymbol{\omega} = \boldsymbol{\omega}^*\delta_m^2/\Gamma\,, \qquad \boldsymbol{B} = \boldsymbol{B}^*\delta_m^2/\Phi \tag{1.4}$$

and, under the assumption of aligned fields,

$$\boldsymbol{\omega} = \omega(r,\theta)\hat{\boldsymbol{z}}\,, \qquad \boldsymbol{B} = B(r,\theta)\hat{\boldsymbol{z}}\,, \tag{1.5a,b}$$

where $\hat{\boldsymbol{z}}$ is a unit vector in the direction Oz. The vorticity and magnetic induction equations then reduce in polar coordinates (cf. MKO94) to the similar form

$$\frac{1}{r}\frac{\partial(\psi,\omega)}{\partial(r,\theta)} = -\epsilon_m(\tilde{\mathrm{L}}_0 + \lambda \mathrm{L}_1)\omega\,, \tag{1.6}$$

$$\frac{1}{r}\frac{\partial(\psi,B)}{\partial(r,\theta)} = -\epsilon_m(\mathrm{L}_0 + \lambda \mathrm{L}_1)B\,, \tag{1.7}$$

where

$$\mathrm{L}_0 = 1 + \tfrac{1}{2}r\frac{\partial}{\partial r} + \nabla^2\,, \tag{1.8a}$$

$$\tilde{\mathrm{L}}_0 = 1 + \tfrac{1}{2}r\frac{\partial}{\partial r} + P_m\nabla^2\,, \tag{1.8b}$$

$$\mathrm{L}_1 = (\tfrac{1}{2}\cos 2\theta)r\frac{\partial}{\partial r} - (\tfrac{1}{2}\sin 2\theta)\frac{\partial}{\partial \theta}\,, \tag{1.8c}$$

and

$$\epsilon_m = \eta/\Gamma \ , \qquad \lambda = \frac{\alpha - \beta}{\alpha + \beta} \, . \tag{1.9}$$

The (non-negative) parameter λ is a measure of the non-axisymmetry of the strain field (1.1); usually we are concerned with the range $0 \leqslant \lambda < 1$; occasionally however we shall discuss the situation $\lambda \geqslant 1$ (equivalently $\beta \geqslant 0$). The parameter ϵ_m is the reciprocal of a magnetic Reynolds number

$$R_m = \epsilon_m^{-1} = \Gamma/\eta \, . \tag{1.10}$$

We first present an asymptotic theory for large R_m,

$$R_m \gg 1 \ , \qquad \text{i.e.} \qquad \epsilon_m \ll 1 \, , \tag{1.11}$$

and then consider the situation when ϵ_m increases to values of order unity and greater.

Note that the Lorentz force associated with the magnetic field (1.5*b*) is irrotational, and therefore makes no contribution to the vorticity equation (1.6) (although it does have an effect on the pressure field). This means that (1.6) is the same as in MKO94, (but with δ_m instead of δ_v used for non-dimensionalization). For $\epsilon = \epsilon_m P_m \ll 1$, and for $r \gg P_m^{-1/2}$, the asymptotic solution of (1.6) obtained by MKO94 has the form

$$\psi(r, \theta) = -\frac{1}{2\pi} \ln r + C \frac{\epsilon_m \lambda P_m^2}{r^2} \sin 2\theta + O\left(\frac{\lambda \epsilon_m^2 P_m^4}{r^4} \right) \tag{1.12}$$

where $C = -17.472\ldots$. Hence, provided $P_m \ll 1$ as assumed here, we have indeed

$$\psi(r, \theta) \sim -\frac{1}{2\pi} \ln r \qquad (r \gg P_m^{1/2}) \tag{1.13}$$

and (1.7) then becomes

$$-\frac{1}{2\pi r^2} \frac{\partial B}{\partial \theta} = -\epsilon_m (\mathrm{L}_0 + \lambda \mathrm{L}_1) B \, . \tag{1.14}$$

This linear equation, deceptively simple in form, is investigated in the following sections of the paper. We require a solution which satisfies the (normalized) flux condition

$$\int_0^\infty \int_0^{2\pi} B(r, \theta) r \mathrm{d}r \mathrm{d}\theta = 1, \tag{1.15}$$

and boundary conditions that $B(r, \theta)$ behaves 'reasonably' (despite the presence of the vortex) as $r \to 0$, i.e.

$$B(r, \theta) = O(1) \qquad \text{as} \qquad r \to 0 \, , \tag{1.16}$$

and that B settles down to the unique (up to a constant b) solution of (1.14) that obtains in the far field where the effect of the vortex is negligible, i.e.

$$\begin{aligned} B(r, \theta) &\sim b \exp\left(\frac{\alpha x^{*2} + \beta y^{*2}}{\eta} \right) = b \exp\left(-\tfrac{1}{4} r^2 (1 + \lambda \cos 2\theta) \right) \\ &= b \mathrm{e}^{-r^2/4} \left(1 - \lambda \tfrac{1}{4} r^2 \cos 2\theta + \tfrac{1}{2} \lambda^2 \left(\tfrac{1}{4} r^2 \right)^2 \cos^2 2\theta + \ldots \right) . \end{aligned} \tag{1.17}$$

Here, we see the need for the assumption $\lambda < 1$ (i.e. $\beta < 0$).

The total velocity field with which we are concerned is that due to the uniform strain (1.1) plus that due to the point vortex (1.13); the dimensionless (r, θ, z) components

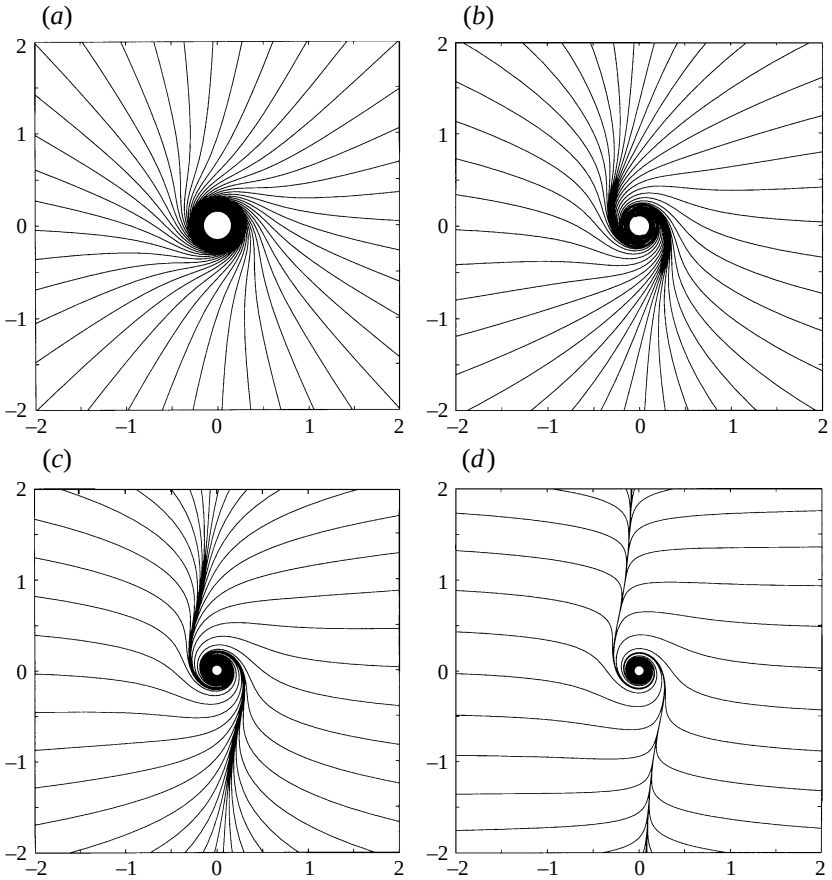

FIGURE 1. The projections of the streamlines of the flow (1.18) on the (x, y) plane with (a) $\lambda = 0$; (b) $\lambda = 0.3$; (c) $\lambda = 0.6$; (d) $\lambda = 0.9$. The scaled radius is $r\epsilon_m^{1/2}$.

of this total velocity field are

$$u_r = -\tfrac{1}{2}\epsilon_m r(1 + \lambda\cos 2\theta)\,, \qquad u_\theta = \frac{1}{2\pi r} + \tfrac{1}{2}\epsilon_m \lambda r \sin 2\theta\,, \qquad u_z = \epsilon_m z\,. \tag{1.18}$$

Note that the scale $(\pi\epsilon_m(1-\lambda))^{-1/2}$ represents the distance from the origin at which the vortex and the strain field have comparable intensities. For $r \ll (\pi\epsilon_m(1-\lambda))^{-1/2}$, the vortex dominates, while for $r \gg (\pi\epsilon_m(1-\lambda))^{-1/2}$, the strain dominates. Figure 1 shows the projection of the streamlines of the velocity field (1.18) on any plane $z = \text{const.}$ for various values of λ; note the increasingly strong convergence towards the axis Oy as λ increases from zero. The scale of the magnetic flux tube is $O(1)$ in the dimensionless units adopted; hence when $\epsilon_m \ll 1$, the flux tube is confined to the region where the vortex dominates; this induces a strong 'axisymmetrization' of the flux tube as we shall see; nevertheless all departures from axisymmetry are induced by the strain field and controlled by a complex interaction of strain, vortex and magnetic diffusion even in the region where $r = O(1)$.

We conclude this introductory section with a plan of the paper. In §2, we recall the asymptotic high-R_m (or low-ϵ_m) theory of Bajer (1995) which is a natural extension of the approach of MKO94. This predicts elliptic structure for the curves $B(r, \theta) = \text{const.}$ with principal axes at 45° inclination to the principal axes of strain (Ox, Oy). The

asymptotic expansion appears to be valid for $r = O(1)$ but fails for $r = O(R_m^{-1/2})$ and in particular fails to satisfy the outer boundary condition (1.17). In §3, we seek to rectify this failing by numerical means. The computed solution does reveal roughly elliptic contours, but the orientation of these contours shows damped oscillations as $r \to 0$ which are not present in the asymptotic solution.

This puzzling behaviour is explained in §4 where we develop an expansion in powers of λ yielding a solution valid uniformly for all r and matching the outer solution (1.17). The expansion reveals a non-analytic part with spiral level contours and validates the numerical results of §3. In order to investigate the convergence of both the asymptotic expansion and the λ-expansion as well as explain the difference between them we derive a family of series solutions in powers of r. The details are given in Appendix A. In §5 we summarize the results.

2. Asymptotic theory for $R_m \gg 1$

As in MKO94, we may seek an asymptotic solution of (1.14) for $\epsilon_m \ll 1$ in the form

$$B = B_0 + \epsilon_m B_1 + \epsilon_m^2 B_2 + \dots . \tag{2.1}$$

At leading order, $\partial B_0/\partial\theta = 0$, so that $B_0 = B_0(r)$, and at higher orders

$$\frac{1}{2\pi r^2}\frac{\partial B_n}{\partial \theta} = (\mathrm{L}_0 + \lambda \mathrm{L}_1)B_{n-1} \qquad (n = 1, 2, 3, \dots). \tag{2.2}$$

Integrating the $n = 1$ equation over θ (from zero to 2π) gives the solvability condition

$$\mathrm{L}_0 B_0(r) = 0 \tag{2.3}$$

with unique solution (satisfying (1.14) and (1.15))

$$B_0(r) = (4\pi)^{-1}\mathrm{e}^{-r^2/4}. \tag{2.4}$$

Equation (2.2) (with $n = 1$) then integrates to give

$$B_1(r,\theta) = -\tfrac{1}{16}\lambda r^4 \mathrm{e}^{-r^2/4}\sin 2\theta\,, \tag{2.5}$$

the arbitrary additive function of r being eliminated by application of the solvability condition at order ϵ_m^2.

Similarly, we may proceed to higher levels, obtaining successively $B_2(r,\theta)$, $B_3(r,\theta)$, $B_4(r,\theta)$, …; thus we find

$$B_2(r,\theta) = -\tilde{\lambda}\pi r^4 \mathrm{e}^{-r^2/4}\left[2(r^2-6)\cos 2\theta + \tilde{\lambda} r^2(r^2-4)\cos 4\theta\right], \tag{2.6}$$

$$\begin{aligned} B_3(r,\theta) = {} & 2\tilde{\lambda}\pi^2 r^4 \mathrm{e}^{-r^2/4}\left[\left((3r^4 - 44r^2 + 72) + \tilde{\lambda}^2 r^4(r^4 - 28r^2 + 80)\right)\sin 2\theta\right. \\ & \left. + \tilde{\lambda} r^2(2r^4 - 29r^2 + 44)\sin 4\theta + \tfrac{1}{3}\tilde{\lambda}^2 r^4(r^4 - 12r^2 + 16)\sin 6\theta\right], \end{aligned} \tag{2.7}$$

$$\begin{aligned} B_4(r,\theta) = {} & \tilde{\lambda}\pi^3 r^4 \mathrm{e}^{-r^2/4}\Big[\Big(8(3r^6 - 78r^4 + 388r^2 - 216) \\ & + 4\tilde{\lambda}^2 r^6(5r^4 - 225r^2 + 2244)\Big)\cos 2\theta \\ & + \big(4\tilde{\lambda} r^2(4r^6 - 111r^4 + 593r^2 - 364) \\ & + \tfrac{8}{3}\tilde{\lambda}^3 r^6(r^6 - 48r^4 + 496r^2 - 832)\big)\cos 4\theta \\ & + \tfrac{4}{9}\tilde{\lambda}^2 r^4(9r^6 - 243r^4 + 1244r^2 - 752)\cos 6\theta \\ & + \tfrac{1}{3}\tilde{\lambda}^3 r^6(r^6 - 24r^4 + 112r^2 - 64)\cos 8\theta\Big], \end{aligned} \tag{2.8}$$

and so on. Here $\tilde{\lambda} = \lambda/16$.

Note that in B_n, the largest power of r is r^{4n} and this appears in conjunction with a factor λ^n; thus, for example, for $\lambda = O(1)$ and $r \gg 1$,

$$B_2(r,\theta) \sim -\pi\tilde{\lambda}^2 r^8 \mathrm{e}^{-r^2/4}\cos 4\theta\,, \tag{2.9a}$$

$$B_3(r,\theta) \sim \tfrac{2}{3}\pi^2\tilde{\lambda}^3 r^{12}\mathrm{e}^{-r^2/4}(3\sin 2\theta + \sin 4\theta)\,, \tag{2.9b}$$

$$B_4(r,\theta) \sim \tfrac{1}{3}\pi^3\tilde{\lambda}^4 r^{16}\mathrm{e}^{-r^2/4}(8\cos 4\theta + \cos 8\theta)\,. \tag{2.9c}$$

The ordering of the terms of (2.1) is thus consistent only if $r \lesssim R_\epsilon$ where

$$R_\epsilon = O(\epsilon_m\lambda)^{-1/4}\,. \tag{2.10}$$

To order ϵ_m, for $r = O(1)$ the contours $B_0 + \epsilon_m B_1 = \text{const.}$ are ellipses inclined at an angle 45° to the principal axes of strain. The manner in which these contours rotate and deform as r increases from $O(1)$ to $O(R_\epsilon)$ is not apparent from the above expansion.

Note finally that the coefficient of terms involving $\sin 2\theta$ or $\cos 2\theta$ in (2.5) and (2.6) are of order r^4 for *small* r, while the coefficient of $\cos 4\theta$ in (2.6) is of order r^6 for small r. This type of behaviour persists at higher order: the coefficients of terms in $\cos 2n\theta$ or $\sin 2n\theta$ are $O(r^{2(n+1)})$ for small r.

3. Uniformly valid solution

The above asymptotic solution has to be regarded at best as an inner solution which must be matched in some way to a solution that satisfies the outer boundary condition (1.17). Let us seek a solution in the form of a Fourier series

$$B(r,\theta) = \sum_{n=-\infty}^{\infty} b_n(r)\mathrm{e}^{\mathrm{i}2n\theta}, \tag{3.1}$$

where, for reality of B,

$$b_{-n}(r) = b_n^*(r)\,, \tag{3.2}$$

the star now representing the complex conjugate. Only terms proportional to $\mathrm{e}^{\mathrm{i}2n\theta}$ occur in (3.1) from the structure of equation (1.14). Substitution in this equation yields a set of coupled linear differential equations:

$$b_n'' + \left(\frac{1}{r} + \tfrac{1}{2}r\right)b_n' + \left(1 - \frac{4n^2}{r^2}\right)b_n + \tfrac{1}{2}\lambda\left[(n+1)b_{n+1} - (n-1)b_{n-1}\right]$$
$$= -\tfrac{1}{4}\lambda r\left(b_{n-1}' + b_{n+1}'\right) + \frac{\mathrm{i}n}{\pi\epsilon_m r^2}b_n \qquad (n = 0, \pm1, \pm2, \ldots). \tag{3.3}$$

We must apply boundary conditions for this set of equations for both $r \to 0$ and $r \to \infty$. Noting the comment at the end of §2, the appropriate conditions for $r \to 0$ are evidently

$$b_0(r) \sim (4\pi)^{-1}\,, \qquad b_n(r) \sim r^{2(n+1)} \qquad (n \geqslant 1) \qquad \text{as } r \to 0\,. \tag{3.4}$$

For $r \to \infty$, the Fourier coefficients are given from (1.17) by

$$b_n(r) \sim \frac{b}{2\pi}\int_0^{2\pi} \mathrm{e}^{-r^2(1+\lambda\cos 2\theta)/4}\mathrm{e}^{-\mathrm{i}2n\theta}\mathrm{d}\theta$$
$$= 2(-1)^n b\,\mathrm{e}^{-r^2/4}I_n(\tfrac{1}{4}\lambda r^2), \tag{3.5}$$

where $I_n(\xi)$ is a modified Bessel function (Gradshtein & Ryzhik 1994) whose asymp-

totic behaviour for n fixed and $\xi \to \infty$ is

$$I_n(\xi) \sim (2\pi\xi)^{-1/2} \mathrm{e}^{\xi}\,. \tag{3.6}$$

Hence, for fixed n,

$$b_n(r) \sim \frac{2^{3/2}(-1)^n b\,\mathrm{e}^{-r^2/4}}{(2\pi\lambda r^2)^{1/2}}\,\mathrm{e}^{\lambda r^2/4} = \left(\frac{8}{\pi\lambda}\right)^{1/2} (-1)^n b r^{-1} \mathrm{e}^{-(1-\lambda)r^2/4}. \tag{3.7}$$

Therefore, when r is large all Fourier coefficients have the same magnitude for n up to about $\frac{1}{4}\lambda r^2$, beyond which a different asymptotic behaviour of I_n becomes valid and $|b_n|$ decreases with n.

In order to solve (3.3) numerically we must impose the boundary condition (3.5) at some finite radius $r = R$. The asymptotic behaviour of $b_n(r)$ shows that the larger we choose R the bigger the number of Fourier modes we have to take into account. However, we must not choose R too small. It must be in the region where the strain dominates and (1.17) is valid, which means $R \gtrsim L = (\pi\epsilon_m(1-\lambda))^{-1/2}$ (cf. 1.18). Taking $R = L$ we can estimate the number of Fourier modes needed:

$$N \approx \tfrac{1}{4}\lambda L^2 = \lambda\,[4\pi(1-\lambda)\epsilon_m]^{-1}\,. \tag{3.8}$$

We solve numerically equations (3.3) using the deferred correction technique (NAG routine D02 GBF) for $N = 20$ modes with the condition (3.4) imposed at $r = r_0 = 10^{-5}$ and (3.5) at $r = R = 10$.

The resulting contours of B and the corresponding contours of the (non-dimensional) ohmic dissipation,

$$D_m = \frac{1}{2}\left(\frac{\partial B_i}{\partial x_j} - \frac{\partial B_j}{\partial x_i}\right)\left(\frac{\partial B_i}{\partial x_j} - \frac{\partial B_j}{\partial x_i}\right), \tag{3.9}$$

are plotted in figures 2–4.

They do not depend on the precise values of r_0, R or N. The contours of B have a maximum at the origin and for smaller values of ϵ_m, e.g. $\epsilon_m = 0.01$ and $\epsilon_m = 0.05$, they seem to be elliptical with 45° inclination, as predicted by the expansion (2.1); farther out they rotate back towards the axes of strain to match the outer solution (1.17).

The contours of the ohmic dissipation D_m show similar change of orientation, but are strongly dipolar with a minimum at the origin (this minimum is to be expected because the current associated with a field given by (3.1) and (3.4) is zero at $r = 0$). The line joining the maxima of D_m is inclined to the axis of weaker strain at an angle $\alpha(\epsilon_m)$. For small ϵ_m the angle $\alpha(\epsilon_m)$ is close to 45° and the contours approach those obtained from the expansion (2.1) (cf. Bajer 1995). For larger values of ϵ_m, i.e. $\epsilon_m = 0.1$ and $\epsilon_m = 1.0$, they do not seem to have the diagonal orientation.

The asymptotic behaviour $b_n \sim r^{2(n+1)}$ as $r \to 0$ implies that the shape of the inner contours is determined by

$$b_0(r) + 2b_1^R(r)\cos 2\theta - 2b_1^I(r)\sin 2\theta \approx \text{const}\,, \tag{3.10}$$

where the superscripts denote the real and imaginary parts. The expansion (2.1) predicts (see (2.5) and (2.6))

$$b_0(r) = \tfrac{1}{4}\pi^{-1}\left(1 - \tfrac{1}{4}r^2 + \tfrac{1}{32}r^4 \ldots\right), \tag{3.11a}$$

$$b_1^R(r) = \tfrac{3}{8}\lambda\epsilon_m^2\pi r^4 + O(\epsilon_m^4), \tag{3.11b}$$

$$b_1^I(r) = \tfrac{1}{32}\lambda\epsilon_m r^4 + O(\epsilon_m^3), \tag{3.11c}$$

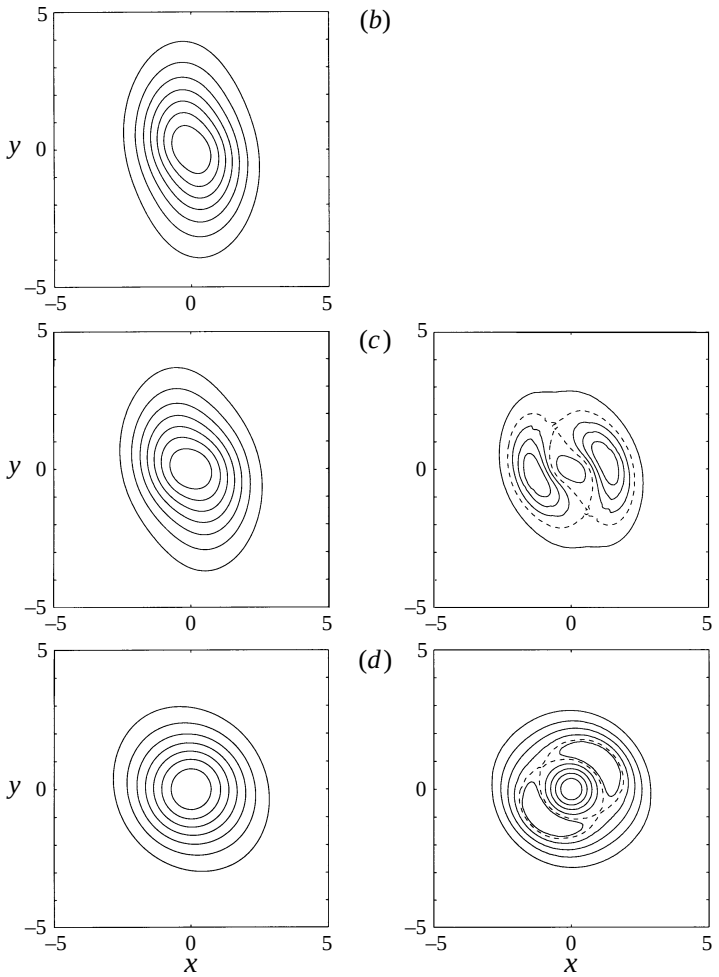

FIGURE 2. Contours of the magnetic field B (left column) and of the ohmic dissipation D_m (right column) with $\lambda = 0.5$ and (*a*) $\epsilon_m = 1.0$; (*b*) $\epsilon_m = 0.1$; (*c*) $\epsilon_m = 0.05$; (*d*) $\epsilon_m = 0.01$.

and so, since $|b_1^I| \ll |b_1^R|$ as $r \to 0$, the inner contours have elliptical shape inclined at 45° to the principal axes of strain.

In figure 5 we show a scaled logarithmic plot of $2b_1^R$ as obtained from a numerical solution. When ϵ_m is smaller than a certain threshold value ϵ_0 somewhere between 0.01 and 0.02 the function $2b_1^R(r)/r^4$ oscillates, but converges to $\frac{3}{8}\lambda\epsilon_m^2\pi$ as $r \to 0$

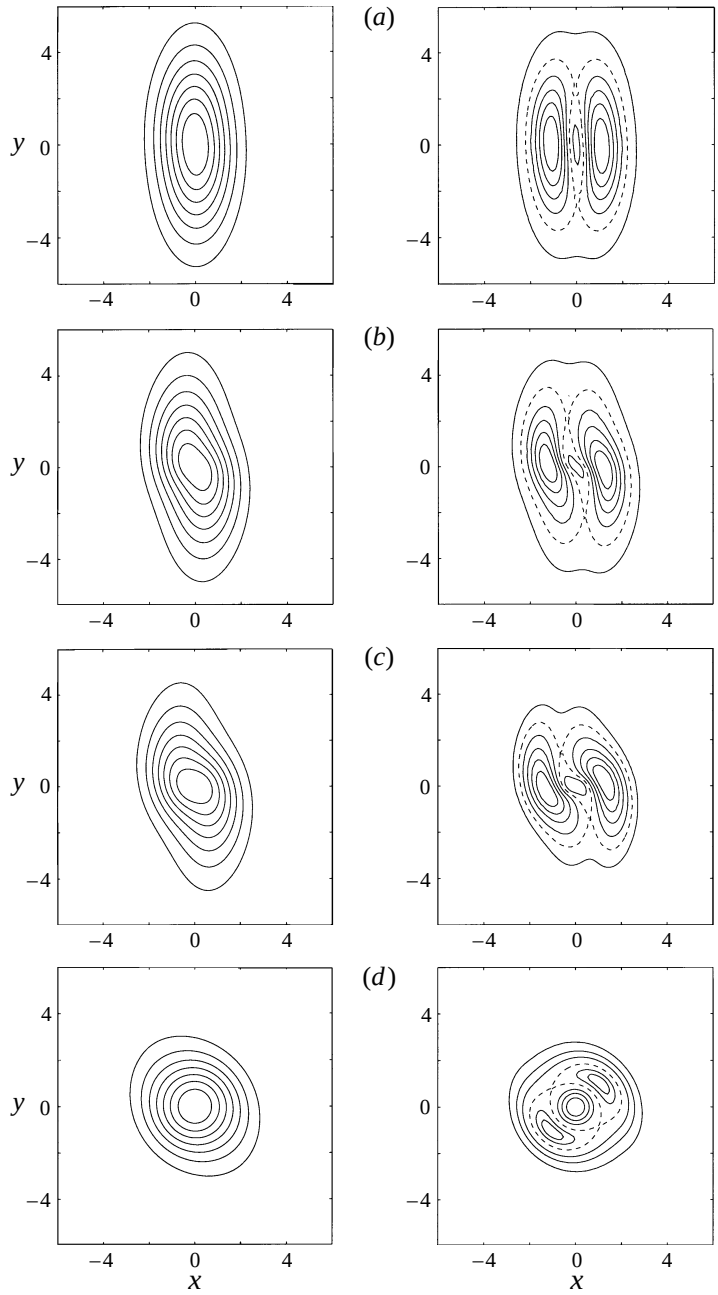

FIGURE 3. Contours of the magnetic field B (left column) and of the ohmic dissipation D_m (right column) with $\lambda = 0.7$ and (*a*) $\epsilon_m = 1.0$; (*b*) $\epsilon_m = 0.1$; (*c*) $\epsilon_m = 0.05$; (*d*) $\epsilon_m = 0.01$.

(figure 5*a*). However, when $\epsilon_m > \epsilon_0$ the function $b_1^R(r)$ looks very different. It seems to have an infinite number of zeros accumulating at $r = 0$ (figure 5*b*). The magnitude of $b_1^R(r)$ decreases like r^p, but the computed value of p (when $\epsilon_m = 0.02$) appears to be $p = 3.19\ldots$ instead of $p = 4$ as in (3.11).

This gives rise to an apparent inconsistency. The computed solution shows different

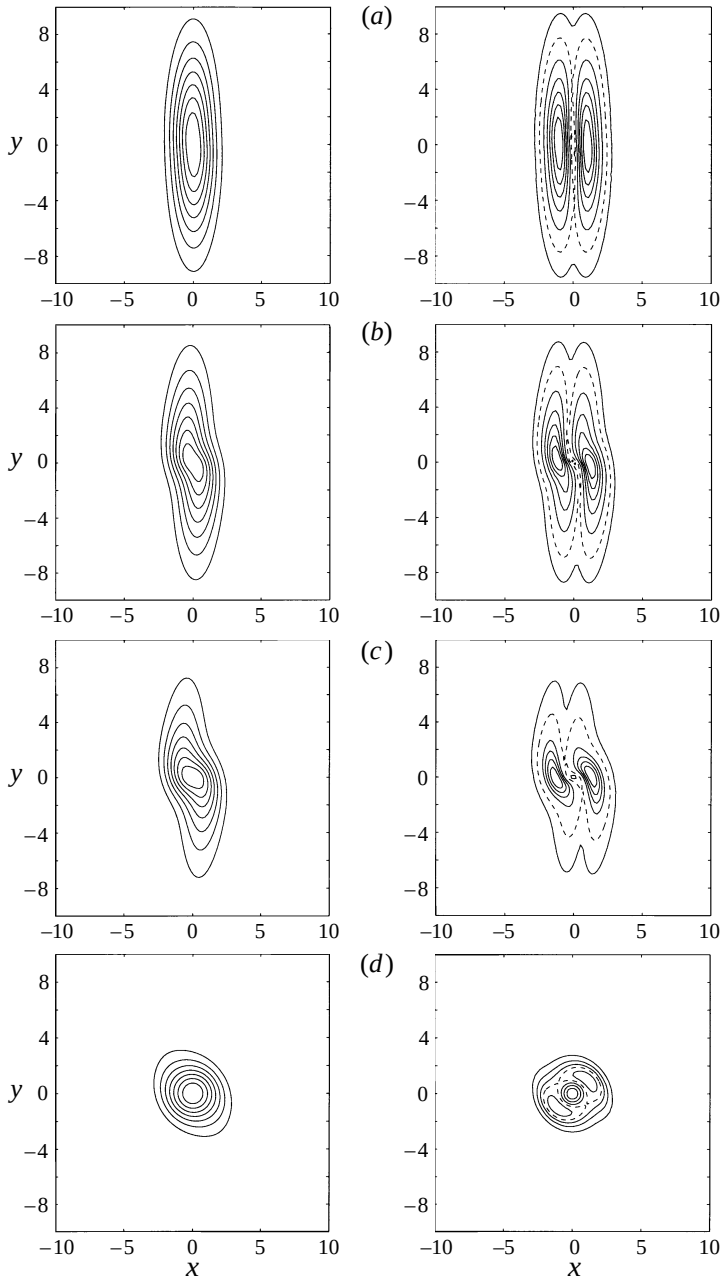

FIGURE 4. Contours of the magnetic field B (left column) and of the ohmic dissipation D_m (right column) with $\lambda = 0.9$ and (*a*) $\epsilon_m = 1.0$; (*b*) $\epsilon_m = 0.1$; (*c*) $\epsilon_m = 0.05$; (*d*) $\epsilon_m = 0.01$.

small-r behaviour from what we assumed (conditions (3.4)) when calculating it. We have tried different boundary conditions at r_0, for example $b_n(r_0) = 0$, and find the same oscillatory behaviour with the same phase, amplitude and value of p. Changing the value of r_0 we find that the boundary condition affects the solution only in a small neighbourhood of r_0. Hence the oscillations seen in figure 5(*b*) are not related to the conditions adopted at r_0.

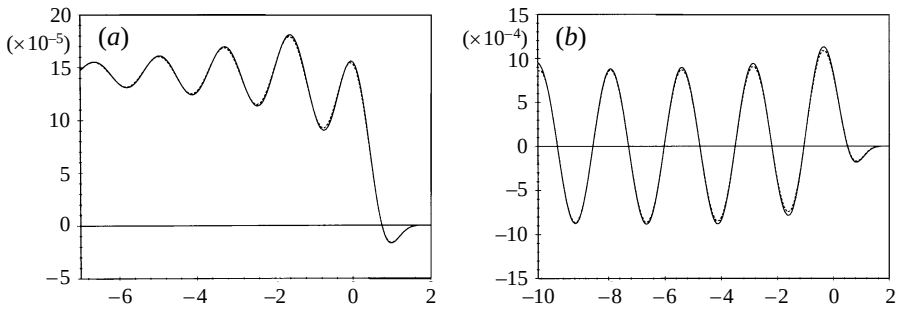

FIGURE 5. $2b_1(r)/r^p$ versus $\ln r$ from a numerical solution of (3.3)–(3.5) (solid line) and from the expansion in powers of λ (dashed line) (see §4) with $N = 10$, $\lambda = 0.7$ and (*a*) $p = 4$, $\epsilon_m = 0.01$; (*b*) $p = 3.19$, $\epsilon_m = 0.02$.

We cannot decide *a priori* on the grounds of the numerical solution alone whether the oscillatory behaviour is or is not a result of truncation of the system (3.3). Truncating at $n = 1$ we obtain two coupled linear equations for b_0 and b_1 which can be manipulated to give a single fifth-order equation for b_0 (see Appendix A),

$$w^4 b_0'''' + (3w^4 + 6w^3) b_0''' + [(K+2)w^4 + 16w^3 + 5w^2] b_0''' + [Kw^4 + (5K+9)w^3 + 12w^2 - w] b_0'' + [(3K+1)w^3 + (3K+6)w^2 - 2w + 1 + \sigma^2] b_0' + [2w^2 - w + 1 + \sigma^2] b_0 = 0, \tag{3.12}$$

where $K = 1 - \frac{1}{2}\lambda^2$, $w = \frac{1}{4}r^2$ is a new variable and

$$\sigma = (4\pi\epsilon_m)^{-1}. \tag{3.13}$$

From any solution $b_0(r)$ we can easily calculate the corresponding $b_1(r)$ satisfying the truncated system. There are two solutions finite at $r = 0$:

$$b_0^1(w) = 1 - w + \tfrac{1}{2}w^2 - \tfrac{1}{6}\left[1 + \frac{3\lambda^2}{9+\sigma^2}\right] w^3 + O(w^4), \tag{3.14a}$$

$$b_1^1(w) = \frac{\frac{1}{2}\lambda}{3 - \mathrm{i}\sigma} w^2 + O(w^3); \tag{3.14b}$$

$$b_0^2 = w^\delta \left[1 + O(w)\right], \tag{3.14c}$$

$$b_1^2 = -\tfrac{1}{2}\lambda w^{\delta-1}\left[\frac{1}{\delta} - \frac{1}{2\delta - 1} w + O(w^2)\right]; \tag{3.14d}$$

where $\delta = 1 + (1 + \mathrm{i}\sigma)^{1/2}$. The general solution of (3.12) finite at $r = 0$ is a linear combination of these two solutions, so the behaviour of $b_1(r)$ as $r \to 0$ depends on the value of δ. When $\delta^R - 1 < 2$, which corresponds to $\epsilon_m > \epsilon_0 = (16\pi\sqrt{3})^{-1} = 0.01148\ldots$, we have

$$b_1(r) \sim r^{2(\delta-1)} = r^{2(\delta^R - 1)} \cos(2\delta^I \ln r + \phi_0), \tag{3.15}$$

ϕ_0 being an arbitrary phase. This is the behaviour observed in figure 5(*b*). Note that when $\epsilon_m = 0.02$, $2(\delta^R - 1) \approx 3.1945\ldots$, very near the value 3.19 obtained in the computation. However, we do not know the asymptotic behaviour of these solutions for $r \to \infty$. The numerical results alone cannot rule out the possibility that these solutions are physically unacceptable as $r \to \infty$. If they decrease rapidly with r it may be necessary to impose the outer boundary condition at very large $r = R$ in order to

filter out the unphysical solutions, i.e. those which do not satisfy (1.17). As explained earlier, this requires a prohibitively large number of Fourier modes.

We show in Appendix A that there are in fact no solutions of (3.12) which satisfy (3.7). This could suggest that the oscillatory behaviour is purely the result of truncation and might disappear when the unphysical solutions are properly filtered out. However, in §4 we develop an expansion in powers of λ which yields a spatially uniform solution and explains the oscillatory behaviour. It has a non-analytic component which is not captured by the asymptotic theory of §2. Near the origin this part vanishes in the limit $\epsilon_m \to 0$, but as ϵ_m increases it becomes more prominent and causes the oscillatory behaviour of the non-axisymmetric Fourier modes, just as seen in figure 5(*b*).

4. Expansion in powers of λ

Let us first rewrite (1.14) in the new coordinates $w = \frac{1}{4}r^2$, $\hat{\theta} = 2\theta$:

$$\frac{\sigma}{w}\frac{\partial B}{\partial \hat{\theta}} = [\mathrm{L}_0 + \lambda \mathrm{L}_1]B, \tag{4.1}$$

where now

$$\mathrm{L}_0 = 1 + w\frac{\partial}{\partial w} + w\left(\frac{\partial^2}{\partial w^2} + \frac{1}{w}\frac{\partial}{\partial w} + \frac{1}{w^2}\frac{\partial^2}{\partial \hat{\theta}^2}\right), \tag{4.2a}$$

$$\mathrm{L}_1 = \cos\hat{\theta} w\frac{\partial}{\partial w} - \sin\hat{\theta}\frac{\partial}{\partial \hat{\theta}}\,. \tag{4.2b}$$

When $\lambda = 0$ the Burgers solution takes a particularly simple form:

$$B^0 = \mathrm{e}^{-w}, \tag{4.3}$$

where, in order to simplify the notation, we now take the total non-dimensional flux to be $\Phi = 4\pi$. With $\lambda = 0$ the equation (4.1) also has a family of non-axisymmetric solutions given by

$$B^N(w,\hat{\theta}) = w^{\beta_N}\mathrm{e}^{-w}\mathrm{e}^{\mathrm{i}N\hat{\theta}/2}F_N(w), \qquad \beta_N = \tfrac{1}{2}N(1 + 2\mathrm{i}\sigma/N)^{1/2}\,, \tag{4.4}$$

where $N = 1, 2, 3, \ldots$, and the F_N are Kummer functions satisfying (Abramovitz & Stegun 1965, §13.1)

$$wF_N'' + (2\beta_N + 1 - w)F_N' - \beta_N F_N = 0. \tag{4.5}$$

These generalize the solutions obtained by Galloway & Zheligovsky (1994) for the pure flux tube problem without a central vortex (i.e. with $\sigma = 0$). The solutions (4.4) have the following asymptotic behaviour:

$$B^N(w,\hat{\theta}) \sim \mathrm{e}^{\mathrm{i}N\theta}w^{\beta_N} \quad \text{as} \quad w \to 0, \tag{4.6a}$$

$$B^N(w,\hat{\theta}) \sim \mathrm{e}^{\mathrm{i}N\theta}w^{-1} \quad \text{as} \quad w \to \infty. \tag{4.6b}$$

The complex power of w in (4.6*a*) means that the level contours near the origin are logarithmic spirals (see figure 6*a* in Appendix A). The solutions are linearly independent and have finite magnetic energy, but $|B^N|$ is not integrable. They have sectors of infinite magnetic flux and cannot be the asymptotic states of the time-dependent problem with finite initial flux. However, Galloway & Zheligovsky (1994) point out that solutions of this kind can play a rôle in direct numerical simulation of the magnetohydrodynamic turbulence.

In Appendix B we analyse the structure of the corresponding family of solutions

of (4.1) when $\lambda \neq 0$. These cannot be written in closed form, rather they are given as power series in w which makes it difficult to analyse their asymptotic behaviour for $w \to \infty$. Rather unexpectedly, they shed light on the nature of the expansion (2.1).

When $\lambda = 0$ all except one solution of (4.4) have non-analytic spiral behaviour near the origin. The physically acceptable one (satisfying (1.17)) is the only exception. When λ is perturbed away from zero there are, in principle, two possible ways in which the family of solutions can be modified. Either the solution satisfying (1.17) is slightly changed, but is still analytic at $r = 0$ and thus exceptional, or all solutions are 'mixed' together and the one satisfying (1.17) acquires a non-analytic spiral component.

We will now show the latter to be true by deriving an expansion in powers of λ:

$$B(w, \hat{\theta}) = \mathscr{B}_0(w) + \lambda \mathscr{B}_1(w, \hat{\theta}) + \lambda^2 \mathscr{B}_2(w, \hat{\theta}) + \ldots. \tag{4.7}$$

Clearly

$$\mathscr{B}_0 = \mathrm{e}^{-w}, \tag{4.8}$$

and the first-order term $\mathscr{B}_1$ can be written as

$$\mathscr{B}_1(w, \hat{\theta}) = \mathrm{Re}(H(w)\mathrm{e}^{\mathrm{i}\hat{\theta}}), \tag{4.9}$$

where the complex function $H(w)$ satisfies the following inhomogeneous linear equation:

$$w^2 H'' + w(w+1)H' + [w - (1 + \mathrm{i}\sigma)]\, H = w^2 \mathrm{e}^{-w}. \tag{4.10}$$

Solutions of the homogeneous equation are

$$H_1(w) = w^\alpha \mathrm{e}^{-w} M(\alpha, 2\alpha + 1, w), \quad H_2(w) = w^\alpha \mathrm{e}^{-w} U(\alpha, 2\alpha + 1, w), \tag{4.11}$$

where $\alpha = \delta - 1 = (1 + \mathrm{i}\sigma)^{1/2}$ and M and U are Kummer's functions (Abramovitz & Stegun 1965, §13.1). $H_1(w)$ and $H_2(w)$ have the following series expansions convergent for all values of w:

$$H_1(w) = w^\alpha \sum_{n=0}^{\infty} C_\alpha^n w^n, \quad H_2(w) = C_+ w^\alpha \sum_{n=0}^{\infty} C_\alpha^n w^n - C_- w^{-\alpha} \sum_{n=0}^{\infty} C_{-\alpha}^n w^n, \tag{4.12}$$

with

$$C_\alpha^n = \frac{\Gamma(2\alpha+1)}{\Gamma(\alpha)} \sum_{k=0}^{n} \frac{(-1)^{n-k}}{k!(n-k)!} \frac{\Gamma(\alpha+k)}{\Gamma(2\alpha+k+1)}, \tag{4.13a}$$

$$C_\pm = \pi\, [\sin \pi(2\alpha+1)\Gamma(\mp\alpha)\Gamma(\pm 2\alpha + 1)]^{-1} = \pm \Gamma(\mp 2\alpha)/\Gamma(\mp\alpha). \tag{4.13b}$$

The solutions have the following asymptotic expansions for large w:

$$H_1(w) \sim \frac{\Gamma(2\alpha+1)}{\Gamma(\alpha)} w^{-1} \left(\sum_{n=0}^{S-1} R_n w^{-n} + O(w^{-S}) \right) + \frac{\Gamma(2\alpha+1)}{\Gamma(\alpha+1)} \mathrm{e}^{\mathrm{i}\pi\alpha} \mathrm{e}^{-w} \left(\sum_{n=0}^{R-1} A_n w^{-n} + O(w^{-R}) \right), \tag{4.14}$$

$$H_2(w) \sim \mathrm{e}^{-w} \left(\sum_{n=0}^{R-1} A_n w^{-n} + O(w^{-R}) \right), \tag{4.15}$$

where

$$A_n = \frac{\Gamma(n+\alpha)\Gamma(n-\alpha)}{\Gamma(\alpha)\Gamma(-\alpha)} \frac{(-1)^n}{n!}, \quad R_n = (-1)^n (n+1)\alpha^{-2} A_{n+1}. \tag{4.16}$$

By means of a Green's function, we construct the unique solution of (4.10) which is finite at $w = 0$ and falls off exponentially when $w \to \infty$:

$$H(w) = -\frac{\Gamma(\alpha)}{\Gamma(2\alpha+1)}\left(H_2(w)\int_0^w \xi H_1(\xi)\,\mathrm{d}\xi + H_1(w)\int_w^\infty \xi H_2(\xi)\,\mathrm{d}\xi\right). \tag{4.17}$$

The series expansion can be obtained from (4.12):

$$H(w) = w^2\sum_{n=0}^{\infty} W_\alpha^n w^n - I_c(\alpha)w^\alpha \sum_{n=0}^{\infty} C_\alpha^n w^n, \tag{4.18}$$

where

$$W_\alpha^n = -\frac{1}{2\alpha}\sum_{k=0}^{n} C_\alpha^k C_{-\alpha}^{n-k}\left[(k+\alpha+2)^{-1} - (n-k-\alpha+2)^{-1}\right],$$

$$I_c(\alpha) = \frac{\Gamma(\alpha)}{\Gamma(2\alpha+1)}\lim_{A\to 0}\left(\int_A^\infty \xi H_2(\xi)\,\mathrm{d}\xi - C_- A^{2-\alpha}\sum_{n=0}^{\infty} C_{-\alpha}^n (n-\alpha+2)^{-1}A^n\right).$$

The expression in brackets becomes independent of A when $A \to 0$, so the limit exists and $I_c(\alpha)$ is finite. When $\mathrm{Re}(\alpha) < 2$ we have (Gradshtein & Ryzhik 1994, §7.621.6)

$$I_c(\alpha) = \frac{\Gamma(\alpha)}{\Gamma(2\alpha+1)}\int_0^\infty \xi H_2(\xi)\,\mathrm{d}\xi = \frac{\Gamma(\alpha)\Gamma(2+\alpha)\Gamma(2-\alpha)}{\Gamma(2\alpha+1)} \neq 0. \tag{4.19}$$

Hence the solution contains a non-analytic component (at least when $\mathrm{Re}(\alpha) < 2$). All orders $\mathscr{B}_1$, $\mathscr{B}_2$, ... of the expansion (4.7) include terms proportional to $\mathrm{e}^{\mathrm{i}2\theta}$, but $\mathscr{B}_1$ dominates as $r \to 0$. Hence, for small r we have (see (3.1), (4.9))

$$b_1(r) \approx \tfrac{1}{2}H(\tfrac{1}{4}r^2). \tag{4.20}$$

In figure 5 we compare $2b_1^R(r)$ computed from the system (3.3) with H^R obtained from (4.17) and find excellent agreement (over the whole range $10^{-5} < r < 10$), which proves that the accumulating zeros of b_1^R are not the result of imperfect computations. It follows that the boundary conditions (3.4) for $b_n(r)$ derived from the high-R_m expansion (2.1) are in fact incorrect, but they have negligible influence on the numerical solution. The expansion (2.1) misses the non-analytic part of the solution because it is proportional to $(\frac{1}{2}r)^{2\alpha}$ and $\mathrm{Re}(\alpha) \sim \epsilon_m^{-1/2}$ for small ϵ_m, so for any fixed $r < 2$ the non-analytic term disappears in the limit $\epsilon_m \to 0$.

The inner contours of $\mathscr{B}_1$ are logarithmic spirals and those of $\mathscr{B}_0 + \lambda\mathscr{B}_1$ have elliptical shape, but the orientation continuously changes when $r \to 0$. The axes of the ellipses lie on a logarithmic spiral, so they do not have definite orientation as $r \to 0$.

Working out the asymptotic series for $H(w)$ when $w \to \infty$ is straightforward but tedious. The result is

$$H(w) \sim -w\mathrm{e}^{-w} + \mathrm{i}\sigma \ln w\,\mathrm{e}^{-w}\sum_{n=0} A_n w^{-n} - \mathrm{e}^{-w}\sum_{n=0} V_n w^{-n}, \tag{4.21}$$

where V_n can be calculated from (4.4) and (4.5). The leading term of $\mathscr{B}_1$ is therefore

$$\mathscr{B}_1 = \mathrm{Re}(H(w)\mathrm{e}^{\mathrm{i}\hat{\theta}}) \sim -w\mathrm{e}^{-w}\cos\hat{\theta}, \tag{4.22}$$

the same as in (1.17).

Comparing (4.8) and (4.22) it may seem that the expansion (4.7) is valid only when

$\lambda w \lesssim 1$. In Appendix B we argue that (4.7) is in fact a convergent series for all values of λ and any fixed r, as is the Taylor series (in powers of λ) of the matching outer solution (1.17).Thus we have obtained a uniformly valid solution of (1.14) satisfying (1.17).

In Appendix B, we also explain the difference between (2.1) and (4.7) in greater detail. We find an analytic (in r) solution which is approximated by (2.1) and a family of non-analytic solutions, analogous to (4.4), which must be added to make a unique solution satisfying (1.17). The expansion (4.7) approximates this unique solution.

In practice convergence of (4.7) is not a useful property. When w is large many terms are needed to obtain a reasonable approximation. It is possible to calculate higher orders, but the results become increasingly more difficult to analyse. Hence, we are rather interested in the region of the (λ, ϵ_m)-space where just the first order, $\mathscr{B}_0 + \lambda\mathscr{B}_1$, is a good approximation. The condition is $|\lambda\mathscr{B}_1| \ll |\mathscr{B}_0|$ which means $r \ll 2\lambda^{-1/2}$ (see (4.8), (4.21)). The approximation will be uniform, provided the radius above which the outer solution is valid, i.e. $r \sim (\pi\epsilon_m(1-\lambda))^{-1/2}$ (see 1.18), is much smaller than $2\lambda^{-1/2}$. We obtain the condition for $\mathscr{B}_0+\lambda\mathscr{B}_1$ to be a good approximation in the entire plane:

$$\lambda \ll \frac{4\pi\epsilon_m}{1+4\pi\epsilon_m} < 1\,. \tag{4.23}$$

We may conclude that the expansion (4.7), although convergent for all values of λ, is useful only when λ is small.

When $\lambda > 1$ we still have a solution, but the matching outer solution (1.17) is unphysical. In fact the problem has no localized steady solution. The streamlines of the flow projected onto the (x, y)-plane have a separatrix and the magnetic flux continuously 'leaks' across the separatrix and is advected away from the origin in a process similar to vortex stripping (Legras & Dritschel 1993). Due to its uniformity in r the λ-expansion shows clearly the disappearance of the steady solution for $\lambda > 1$. It is not the case with the asymptotic theory of §2.

In an interesting way the expansion (4.7) leads to conclusions about convergence of (2.1). From (4.18) we notice that $H(w)$ regarded as function of R_m has singularities in the plane of complex R_m where the denominators of the coefficients W_α^n have zeros. They are all located on the imaginary axis and their position is given by

$$j - \alpha + 2 = 0; \qquad j = 0, 1, 2, \ldots, \tag{4.24}$$

or in terms of R_m,

$$R_m = -\mathrm{i}4\pi(j^2 + 4j + 3). \tag{4.25}$$

The singularities extend to infinity, i.e. there are singularities with arbitrary large absolute value. Hence, the expansion of the function $H(w)$ in powers of $\epsilon_m = {R_m}^{-1}$ is an asymptotic series with zero radius of convergence and the same applies to the expansion (2.1).

The singularity which is closest to the origin in the plane of complex R_m corresponds to $j = 0$ or $R_m = -12\mathrm{i}\pi$. When $R_m \ll 1$ a solution to (1.14)–(1.17) can be sought in the form of a series in powers of R_m. Such series would have finite radius of convergence R_m^0 determined by the nearest singularity. At $O(\lambda)$ we obtain an upper bound $R_m^0 = 12\pi$, but higher orders bring more singularities. In Appendix B we argue that the singularities have an accumulation point at $R_m = -8\mathrm{i}\pi$, thus giving $R_m^0 = 8\pi$.

A low-Reynolds-number theory of this kind was derived by Robinson & Saffman (1984) for the stretched vortex problem. They found no evidence of the radius of convergence being finite. The existence of singularities and their location is an open

problem. It is possible that they are a consequence of the singular flow due to a point vortex in our present problem and that they do not appear in the problem considered by Robinson & Saffman. However, a more likely explanation is that their existence was obscured by the double expansion both in Reynolds number and in the parameter λ.

5. Summary

In this paper we have analysed a rectilinear magnetic sinew strained by non-axisymmetric irrotational ambient flow. A large-R_m expansion was developed by Bajer (1995) for two regimes: $R_\Gamma \gg 1$, $P_m \gtrsim 1$; and $P_m \ll 1$. The value of P_m in the solar convection zone varies from 10^{-5} at the base of the photosphere to 10^2 deeper down (Priest 1982, §1.3.1), so both regimes are of potential interest.

Here we considered in detail the regime when $P_m = R_m/R_\Gamma \ll 1$ The vortex was approximated by a line vortex which corresponds to taking the limit $P_m \to 0$ and neglecting non-axisymmetric terms in the multipole expansion of the velocity.

The expansion (2.1) does not match the linear outer solution. In order to bridge the gap between the two we calculated numerically a uniformly valid solution. When ϵ_m exceeds a certain threshold value the computed asymptotic behaviour as $r \to 0$ of the higher Fourier modes differs essentially from that predicted by the high-R_m expansion. They have an infinite number of zeros accumulating at $r = 0$, a signature of spiral behaviour.

The main result of the paper is the proof that the computations are quantitatively correct and the high-R_m expansion has a rather subtle deficiency, difficult to predict in advance, which becomes prominent when R_m is below a certain threshold. The first indication came from the analysis of the severely truncated system including only two Fourier modes. It reproduced the computational results and gave an accurate threshold value $R_m \approx 87$ (corresponding to $\epsilon_m = 0.01148$), but the solutions had wrong behaviour for $r \to \infty$. In a special case, $\lambda = 0$, we have found an infinite family (4.4) of solutions which are oscillatory near the origin, but they are all excluded by the boundary condition (1.17).

The decisive argument showing that this is not the case when $\lambda > 0$ came from the expansion in powers of λ which yielded a solution valid uniformly in r and satisfying the boundary condition (1.17). The solution validates the numerical results and reveals a non-analytic spiral part which was missing from the large-R_m expansion (2.1). This spiral ingredient is present however large R_m may be, but it becomes weaker as R_m increases relative to the non-oscillatory ingredient.

It is difficult to carry out the procedure to orders higher than $O(\lambda)$, so its practical use is limited to small values of λ, but it reveals the nature of the uniformly valid solution. It appears to be a combination of solutions B^N, analogous to (4.4), the details of which are given in Appendix B. When expanded in powers of ϵ_m these solutions yield divergent asymptotic series. The series corresponding to B^0 appears to be identical with (2.1).

The λ-expansion, together with the matching outer solution (1.17), provide a complete solution to our problem. It shows that the spiral component is indeed present in the steady state. This is different from the unsteady algebraic spirals continuously developing in two-dimensional (Gilbert 1988) and three-dimensional (Lundgren 1982) turbulence.

We expect the magnetic sinews considered here to be prominent features in any physical situation where the magnetic field is weak and passive enough not to prevent

the formation of the coherent vortices. By analogy with the small-scale structures of turbulence such magnetic sinews are likely to feature in weak-field MHD turbulence. Numerical simulations of Brandenburg and others (see Brandenburg 1994) show alignment of $\boldsymbol{B}$ and $\boldsymbol{\omega}$ in some regions and magnetic flux tubes are seen (Brandenburg, Procaccia & Segel 1995), but the magnetic sinews still remain to be properly identified.

We thank Andrew Gilbert and Steve Tobias for helpful comments. This work was supported by PPARC grant no J27974.

Appendix A. Truncated system

Here we derive the equation (3.12) and analyse the asymptotic behaviour of its solutions for $r \to 0$ as well as $r \to \infty$.

Let us consider the lowest non-trivial truncation of (3.3) retaining only b_0 and b_1. Using the variable $w = \frac{1}{4}r^2$ we obtain two equations:

$$w\ddot{b}_0 + (w+1)\dot{b}_0 + b_0 + \lambda(b_1^R + w\dot{b}_1^R) = 0, \tag{A 1a}$$

$$w\ddot{b}_1 + (w+1)\dot{b}_1 + (1-(1+\mathrm{i}\sigma)w^{-1})b_1 + \tfrac{1}{2}\lambda w\dot{b}_0 = 0. \tag{A 1b}$$

We integrate (A 1*a*) once, assuming b_0 to be finite at $w = 0$, and write separately the real and imaginary parts of (A 1*b*),

$$\dot{b}_0 + b_0 + \lambda b_1^R = 0, \tag{A 2a}$$

$$w\ddot{b}_1^I + (w+1)\dot{b}_1^I + (1-w^{-1})b_1^I - \sigma w^{-1}b_1^R = 0, \tag{A 2b}$$

$$w\ddot{b}_1^R + (w+1)\dot{b}_1^R + (1-w^{-1})b_1^R + \sigma w^{-1}b_1^I + \tfrac{1}{2}\lambda w\dot{b}_0 = 0. \tag{A 2c}$$

From (A 2*a*) we have $b_1^R = -\lambda^{-1}(b_0 + \dot{b}_0)$ and then (A 2*c*) gives b_1^I in terms of b_0 and its derivatives. Substituting for b_1^R and b_1^I in (A 2*b*) we obtain equation (3.12).

We look for a series solution of (3.12),

$$b_0(w) = w^{\delta}\sum_{n=0}^{\infty} A_n w^n, \tag{A 3}$$

and obtain two solutions finite at $w = 0$, (3.14*a*) and (3.14*c*). Then the corresponding functions $b_1(w)$ can easily be calculated from (A 1*b*).

The solution (3.14*c*, *d*) has $b_1(w)$ bigger than $b_0(w)$ as $w \to 0$, contrary to the assumption underlying the truncated system. However, the general solution of (3.12) is a combination of (3.14*a*, *b*) and (3.14*c*, *d*), so it has the correct ordering, i.e. $b_1/b_0 \to 0$ as $w \to 0$.

In figure 6(*a*) we show the inner contours of the solution (3.14*c*, *d*) for $\epsilon_m = 0.2$, as given by

$$\mathrm{Re}\left(w^{\delta-1}\mathrm{e}^{\mathrm{i}2\theta}\right) = w^{\delta^{\mathrm{R}}-1}\sin\left(\delta^{\mathrm{I}}\ln w + 2(\theta-\theta_0)\right) = \mathrm{const}, \tag{A 4}$$

where θ_0 is an arbitrary phase. The contours are 'tongues' divided by four separatrices which are logarithmic spirals given by

$$\theta - \theta_0 = -\tfrac{1}{2}\delta^I \ln w + \Psi, \qquad \Psi = 0, \tfrac{1}{2}\pi, \pi, \tfrac{3}{2}\pi. \tag{A 5}$$

In figure 6(*b*) we show the inner contours of the sum of both solutions (3.14). Any linear combination can be reduced to such a sum by an appropriate scaling of w. The contours are given by

$$w + \mathrm{Re}\left(w^{\delta-1}\mathrm{e}^{\mathrm{i}2\theta}\right) = w^{\delta^R-1}\sin\left(\delta^I \ln w + 2(\theta-\theta_0)\right) = \mathrm{const}. \tag{A 6}$$

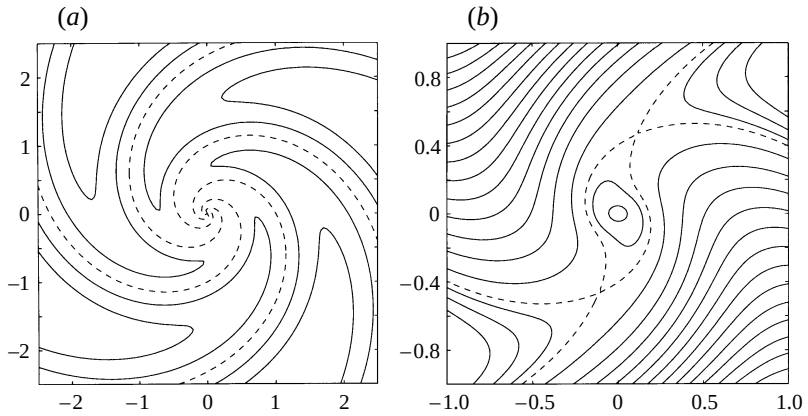

FIGURE 6. Contours of the leading term of the solution (3.13). (*a*) Solution (3.13*c*, *d*) for $\epsilon_m = 0.2$. The radial coordinate is stretched by a transformation $\widetilde{w} \to \widetilde{w}^3$ to emphasize the spiral structure; (*b*) linear combination of both solutions (3.13) for $\epsilon_m = 0.015$. Dashed lines mark the separatrices.

Near the origin they are closed quasi-elliptical curves. The endpoints of the axes of the elipses lie on a logarithmic spiral

$$\delta^I \ln w + 2(\theta - \theta_0) = \pi/2, \tag{A 7}$$

so the contours do not have definite orientation in the limit $w \to 0$ as they had in the solution (2.4)–(2.8).

The two solutions (3.14) have finite flux, energy and dissipation for small r, so they are physically acceptable near the origin. Systematic analysis of (3.12) (see Ince 1956, §§17.5–6, 18.21) shows that there are five solutions with the following asymptotic behaviour for large w:

$$w^{-2}, \quad w^{-2/(2-\lambda^2)}, \quad w^{-2}\exp(-w), \quad w^{\pm\lambda/2(\sqrt{2}\mp\lambda)}\exp[(-1 \pm \lambda/\sqrt{2})w]. \tag{A 8}$$

None of these matches the outer solution (1.17). Hence, the $w \to \infty$ asymptotic behaviour will be modified as the truncation order is increased and thus the asymptotic behaviour as $w \to 0$ could be modified as well. However, in §4 we have shown that the non-analytic spiral part of the solution remains.

Appendix B. Expansion in powers of r

We seek solutions of (4.1) in the form of a series in powers of $w = \frac{1}{4}r^2$,

$$B(w, \hat{\theta}) = w^{\beta} \sum_{n=0}^{\infty} B_n(\hat{\theta}) w^n. \tag{B 1}$$

Both β and B_n are complex numbers, so taking the real part of the right-hand side of the equation is implicitly understood. Substituting in (4.1) we obtain a differential recurrence relation

$$B_n'' - \sigma B_n' + (n+\beta)^2 B_n = \lambda \sin\hat{\theta}\, B_{n-1}' - (n+\beta)B_{n-1} - \lambda(n+\beta-1)\cos\hat{\theta}\, B_{n-1}. \tag{B 2}$$

When $n = 0$ this is an indicial equation

$$B_0'' - \sigma B_0' + \beta^2 B_0 = 0, \qquad B_0(\hat{\theta} + 4\pi) = B_0(\hat{\theta}), \tag{B 3}$$

which gives a family of solutions for the index β,

$$\beta = \beta_N = \tfrac{1}{2}N\left(1 + 2\mathrm{i}\sigma/N\right)^{1/2}, \tag{B 4a}$$

$$B_0 = B_0^N = \text{const} \times \mathrm{e}^{\mathrm{i}N\hat{\theta}/2}; \qquad N = 0, 1, 1, \ldots . \tag{B 4b}$$

We can now solve (B 2) by taking

$$B_n^N(\hat{\theta}) = \sum_{k=-n}^{n} b_{n,k}^N \exp[\mathrm{i}(k + \tfrac{1}{2}N)\hat{\theta}], \tag{B 5}$$

and obtain a recurrence relation for the coefficients $b_{n,k}^N$,

$$\begin{aligned}\left[(n+\beta_N)^2 - (\tfrac{1}{2}N + k)^2 - \mathrm{i}\sigma(\tfrac{1}{2}N + k)\right] b_{n,k}^N \\ = \tfrac{1}{2}\lambda[(\tfrac{1}{2}N + k) - (n + \beta_N)]b_{n-1,k-1}^N - (n+\beta_N)b_{n-1,k}^N - \tfrac{1}{2}\lambda[(\tfrac{1}{2}N + k) + (n+\beta_N)]b_{n-1,k+1}^N.\end{aligned} \tag{B 6}$$

Thus we have a family of solutions,

$$B^N(w, \hat{\theta}) = w^{\beta_N} \sum_{n=0}^{\infty} \left[\sum_{k=-n}^{n} b_{n,k}^N \exp(\mathrm{i}(\tfrac{1}{2}N + k)\hat{\theta})\right] w^n, \tag{B 7}$$

where $b_{0,0}^N$ are arbitrary and $b_{n,k}^N$ are given by (B 6).

The contours of the (real part) of B^N near the origin are logarithmic spirals (except when $N = 0$). In particular, in $B^2(w, \hat{\theta})$ we find the same behaviour we had in the truncated system. The solution $N = 0$ is real and, up to a constant factor, it takes the form:

$$B^0(r, \theta) = 1 - \tfrac{1}{4}r^2 + \left(\frac{3\lambda}{9 + \sigma^2}\cos 2\theta + \tfrac{1}{2} - \frac{\sigma\lambda}{9+\sigma^2}\sin 2\theta\right)\tfrac{1}{16}r^4 \ldots . \tag{B 8}$$

When we expand the coefficients of r^4 in powers of ϵ_m we find that for small ϵ_m (B 8) is the same as the expansion (2.1). We will show later that (B 8) is a convergent series at least when

$$r < \left(\pi(\lambda + \tfrac{1}{2})\epsilon_m\right)^{-1/2}. \tag{B 9}$$

Hence, we have a solution of (1.14) valid for any value of ϵ_m and convergent for $r \lesssim \epsilon_m^{1/2}$ which seems to be the same as (2.1) when ϵ_m is small.

From (B 8) we can see that B^0 regarded as a function of ϵ_m has a singularity at $\sigma = \pm 3\mathrm{i}$, or $\epsilon_m = \pm(12\pi\mathrm{i})^{-1}$. From the recursion relation (B 6) we can easily calculate *all* singularities of B^0. First we notice that $b_{n,n}^0 = b_{n,-n}^0 = 0$. Second, the coefficients $b_{n,k}^0$ have factors

$$(n^2 - k^2 - \mathrm{i}\sigma k)^{-1}, \qquad -n + 1 \leqslant k \leqslant n - 1, \tag{B 10}$$

so they have singularities at

$$\sigma = \pm\mathrm{i}(n^2 - k^2)/k, \qquad k = \pm 1, \pm 2, \ldots, \pm(n-1). \tag{B 11}$$

These singularities lie outside a circle $|\sigma| = 2$ on which they have an accumulation point at $\sigma = \pm 2\mathrm{i}$, but they extend to infinity, as their absolute value has no upper bound. It means that the expansion of B^0 in powers of ϵ_m, apparently identical with (2.1), is an asymptotic series with zero radius of convergence. The fact that the disc $|\sigma| \leqslant 2$ contains no singularities tells us that a *low*-R_m expansion of B^0, i.e. one in powers of R_m, converges for $R_m < 8\pi$.

The λ-expansion of §4 shows that the solution of (1.14) satisfying (1.17) is a combination of the series solutions $B^N(w,\theta)$ with different N. The $O(\lambda)$ term reveals $B^0(w,\theta)$ and $B^2(w,\theta)$. Higher orders in λ presumably bring in solutions with higher N. All the series solutions are analytical functions of λ, so we may expect their combination to be analytical too. Hence, the series (4.7) is convergent for all values of λ.

The solution B^0 determines the shape of the inner contours of $B(r,\theta)$, provided $\mathrm{Re}(\beta_2) > 2$ which means $\sigma > 4\sqrt{3}$ or $\epsilon_m < 0.011\ldots$. Equation (B 8) tells us that these contours have quasi-elliptical shape inclined at an angle α for which we obtain an explicit formula:

$$\tan 2\alpha = -\tfrac{1}{6}\sigma = -(24\pi\epsilon_m)^{-1}. \tag{B 12}$$

Clearly $\alpha \to 45^\circ$ as $\epsilon_m \to 0$, as predicted by the asymptotic expansion (2.1).

Finally we derive the estimate (B 9) for the radius of convergence of (B 8). When $N = 0$ the recurrence relation (B 6) gives an inequality:

$$|b_{n,k}| \leqslant \left|\frac{\lambda(k-n)}{n^2-k^2-\mathrm{i}\sigma k}\right| |b_{n-1,k-1}| + \left|\frac{n}{n^2-k^2-\mathrm{i}\sigma k}\right| |b_{n-1,k}| + \left|\frac{\lambda(k+n)}{n^2-k^2-\mathrm{i}\sigma k}\right| |b_{n-1,k+1}|, \tag{B 13}$$

where, to simplify notation, we drop the superscript ^{0}. Now we take a sum over k,

$$S_n = \sum_{k=-n}^{n} |b_{n,k}| \leqslant \sum_{k=-n+1}^{n-1} \left(\frac{|\frac{1}{2}\lambda(k+1-n)|}{|n^2-(k+1)^2-\mathrm{i}\sigma(k+1)|} + \frac{n}{|n^2-k^2-\mathrm{i}\sigma k|} + \frac{|\frac{1}{2}\lambda(k-1+n)|}{|n^2-(k-1)^2+\mathrm{i}\sigma(k-1)|} \right) |b_{n-1,k}|, \tag{B 14}$$

and use simple estimates,

$$|\tfrac{1}{2}\lambda(k \pm 1 \mp n)| \leqslant \lambda n \qquad \text{for} \qquad n > 0, \tag{B 15a}$$

$$|n^2-k^2-\mathrm{i}\sigma k| \geqslant n\sigma \qquad \text{for} \qquad n \geqslant \tfrac{1}{2}(1+\sigma^2), \tag{B 15b}$$

where $-n \leqslant k \leqslant n$. Hence, we have

$$S_n \leqslant \frac{2\lambda+1}{\sigma} S_{n-1} \qquad \text{for} \qquad n \geqslant \tfrac{1}{2}(1+\sigma^2). \tag{B 16}$$

This implies convergence of (B 7) when $w < \sigma/(2\lambda+1)$ which is the lower bound (B 9).

Similar analysis of convergence can be carried out for other series solutions B^N with $N > 0$. The lower bounds for the radii of convergence are

$$R^N > 2|2\beta_N - N - \mathrm{i}\sigma|^{1/2}(2\lambda+1)^{1/2}. \tag{B 17}$$

Having only the lower bounds we cannot tell whether the series are convergent for large r. We have analysed them using Domb–Sykes plots (Hinch 1991, p. 145). They seem to converge for all values of r, but their asymptotic behaviour could not be confidently determined.

However, each series solution (B 7) provides accurate conditions for all Fourier modes as $r \to 0$, so the system (3.3) can be solved numerically as an initial value problem. We show a sample of the results for $N = 2$ in figure 7. Such a solution is not 'contaminated' by any outer boundary condition. It shows that for large r the solutions (B 7) have an algebraic behaviour,

$$B(r,\theta) \sim r^{-p(\theta)}. \tag{B 18}$$

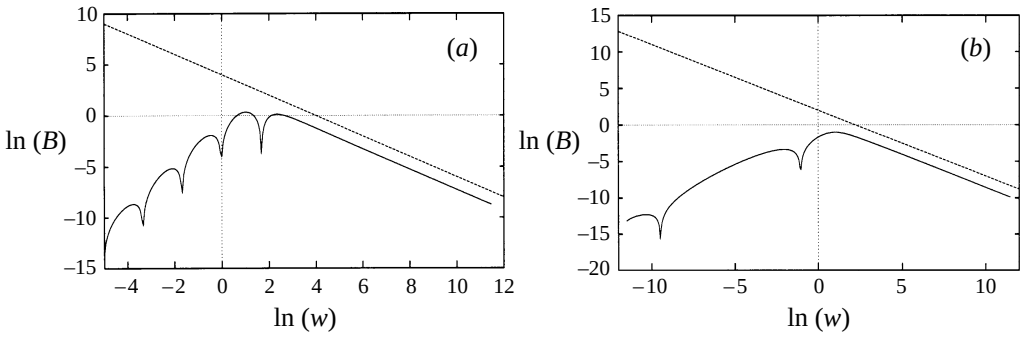

FIGURE 7. Plots of $\ln(B^2(w,\theta=0))$ versus $\ln w$ obtained by solving an initial value problem for (3.3). (*a*) $\lambda = 0$, $\epsilon_m = 0.01$, dashed line corresponds to $B^2(w,0) \sim w^{-1}$; (*b*) $\lambda = 0.1$, $\epsilon_m = 0.1$, dashed line corresponds to $B^2(w,0) \sim w^{-0.9}$.

When $\lambda = 0$ we obtain $p(\theta) = 1$ (see figure 7*a*), in agreement with (4.6*b*). When $\lambda > 0$ we find $p(\theta) < 1$ for some values of θ (figure 7*b*), so the solutions (B 7) have sectors of infinite flux. The physically acceptable solution of (4.1) is a combination of the series solutions (B 7). The coefficients of this combination can, in principle, be determined from the λ-expansion.

REFERENCES

ABRAMOWITZ, M. & STEGUN, I. A. 1965 *Handbook of Mathematical Functions*. Dover.

BAJER, K. 1995 High Reynolds number vortices with magnetic field in non-axisymmetric strain. In *Small-Scale Structures in Three-Dimensional Hydro and Magnetohydrodynamic Turbulence* (ed. M. Meneguzzi, A. Pouquet & P. L. Sulem). Lecture Notes in Physics, vol. 462, pp. 255–264. Springer.

BATCHELOR, G. K. 1950 On the spontaneous magnetic field in a conducting liquid in turbulent motion. *Proc. R. Soc. Lond.* A **201**, 405–416.

BATCHELOR, G. K. 1953 *The Theory of Homogeneous Turbulence*. Cambridge University Press.

BRANDENBURG, A. 1994 Solar dynamos: computational background. In *Lectures on Solar and Planetary Dynamos* (ed. M. R. E. Proctor & A. D. Gilbert), pp. 117–159. Cambridge University Press.

BRANDENBURG, A., PROCACCIA, I. & SEGEL, D. 1995 The size and dynamics of magnetic flux structures in magnetohydrodynamic turbulence. *Phys. Plasmas* **2**, 1148–1156.

BURGERS, J. M. 1948 A mathematical model illustrating the theory of turbulence. *Adv. Appl. Mech.* **1**, 171–199.

CADOT, O., DOUADY S. & COUDER, Y. 1995 Characterisations of the low pressure filaments in a 3D turbulent shear flow. *Phys. Fluids* **7**, 630–646.

DOUADY, S., COUDER, Y. & BRACHET, M. E. 1991 Direct observation of the intermittency of intense vorticity filaments in turbulence. *Phys. Rev. Lett.* **67**, 983–986.

GALLOWAY, D. J. & ZHELIGOVSKY, V. A. 1994 On a class of non-axisymmetric flux rope solutions to the electromagnetic induction equation. *Geophys. Astrophys. Fluid Dyn.* **76**, 253–264.

GILBERT, A. D. 1988 Spiral structures and spectra in two-dimensional turbulence. *J. Fluid Mech.* **193**, 475–497.

GRADSHTEIN, I. S. & RYZHIK, I. M. 1994 *Table of Integrals, Series, and Products*, 5th Edn. Academic Press.

HINCH, E. J. 1991 *Perturbation Methods*. Cambridge University Press.

INCE, E. L. 1956 *Ordinary Differential Equations*. Dover.

JIMÉNEZ, J., MOFFATT, H. K. & VASCO, C. 1996 The structure of the vortices in freely decaying two-dimensional turbulence. *J. Fluid Mech.* **313**, 209–222.

JIMÉNEZ, J., WRAY, A. A., SAFFMAN, P. G. & ROGALLO, R. S. 1993 The structure of intense vorticity in homogeneous isotropic turbulence. *J. Fluid Mech.* **255**, 65–90.

Kida, S. & Ohkitani, K. 1992 Spatio-temporal intermittency and instability of a forced turbulence. *Phys. Fluids* A **4**, 1018–1027.

Legras, B. & Dritschel, D. 1993 Vortex stripping and the generation of high vorticity gradients in two-dimensional flows. *Appl. Sci. Res.* **51**, 445–455.

Lundgren, T. S. 1982 Strained spiral vortex model for turbulent fine structure. *Phys. Fluids* **25**, 2193–2203.

McWilliams, J. C. 1984 The emergence of isolated coherent vortices in turbulent flow. *J. Fluid Mech.* **146**, 21–43.

Moffatt, H. K. 1978 *Magnetic Field Generation in Electrically Conducting Fluids.* Cambridge University Press.

Moffatt, H. K., Kida, S. & Ohkitani, K. 1994 Stretched vortices – the sinews of turbulence; large-Reynolds-number asymptotics. *J. Fluid Mech.* **259**, 241–264 (referred to herein as MKO94).

Priest, E. R. 1982 *Solar Magnetohydrodynamics.* Reidel.

Robinson, A. C. & Saffman, P. G. 1984 Stability and structure of stretched vortices. *Stud. Appl. Maths* **70**, 163–181.

She, Z.-S., Jackson, E. & Orszag, S. A. 1990 Intermittent vortex structures in homogeneous isotropic turbulence. *Nature* **344**, 226–228.

Townsend, A. A. 1951 On the fine-scale structure of turbulence. *Proc. R. Soc. Lond.* A **208**, 534–542.

Villermaux, E., Sixou, B. & Gagne, Y. 1995 Intense vortical structures in grid-generated turbulence. *Phys. Fluids* **7**, 2008–2013.

Vincent, A. & Meneguzzi, M. 1991 The spatial structure and statistical properties of homogeneous turbulence. *J. Fluid Mech.* **225**, 1–25.